Earthquake ruptures and topography controlled by plate interface deformation

Nadaya Cubas[1,*], Philippe Agard[1], and Roxane Tissandier[2]

[1]Sorbonne Universite, CNRS-INSU, Institut des Sciences de la Terre Paris, ISTeP UMR 7193, F-75005 Paris, France
[2]Institut de Physique du Globe de Paris, Université de Paris, CNRS, 75238 Paris, France
[*]nadaya.cubas@sorbonne-universite.fr

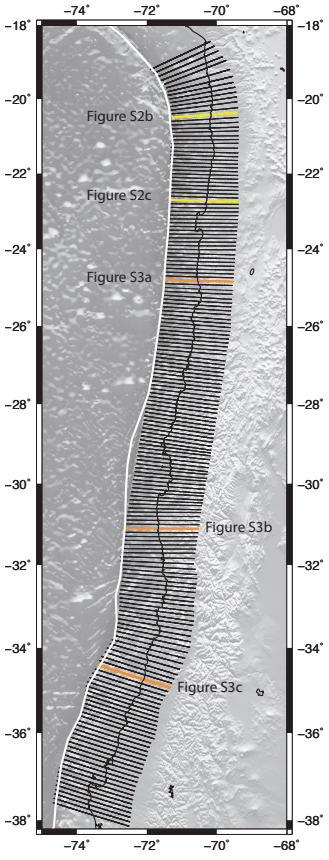

Figure 1: **S1 -** Cross-sections used for inversion.

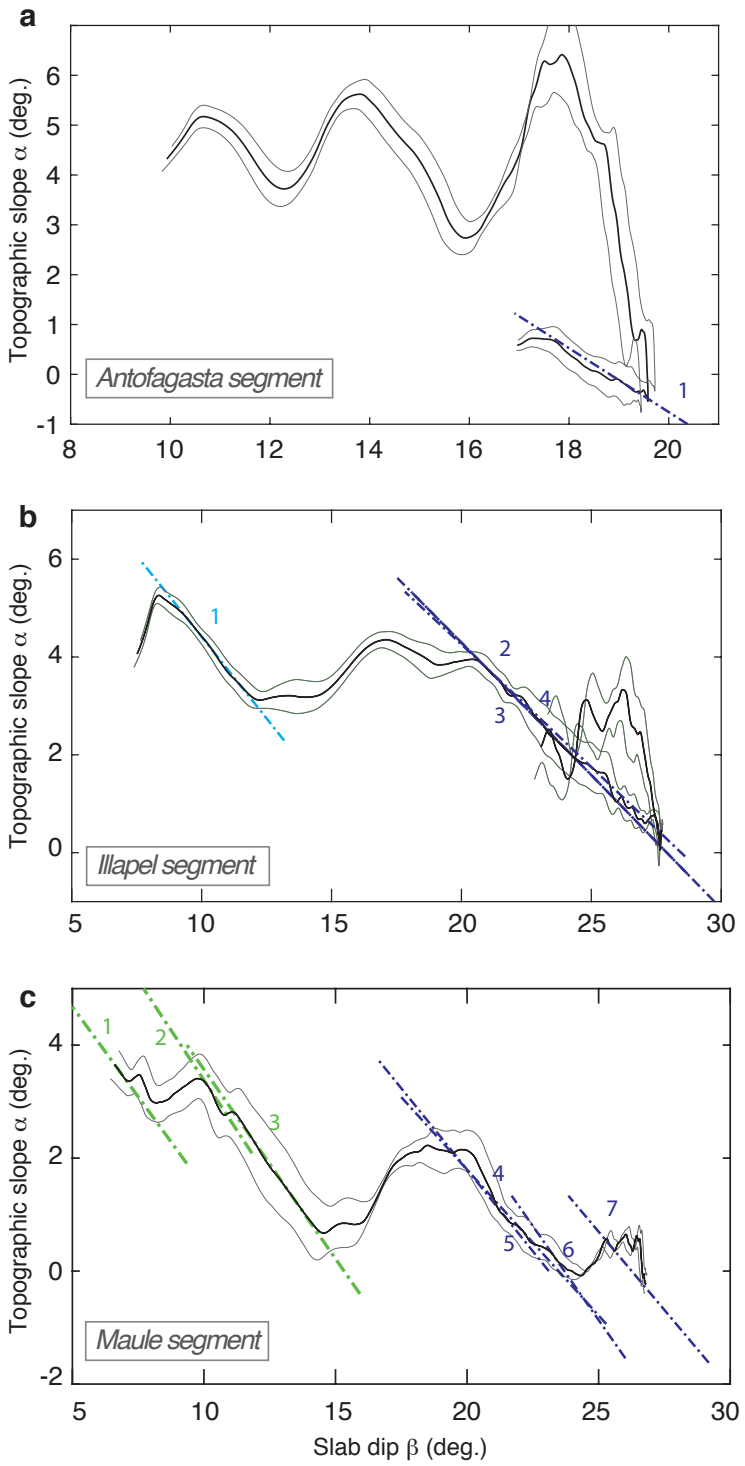

Figure 2: **S2 -** Topographic slope (α) versus slab dip (β) for swath profiles along the a. Antofagasta, b. Illapel and c. Maule segments (locations on Figure **S1**). Segments at critical state, according to inversion, are shown in green: when accretion, in blue: light blue when probably erosive, dark blue for probable underplating. Grey: swath plus or minus standard deviation. Properties of each segment are provided in Table **T1**.

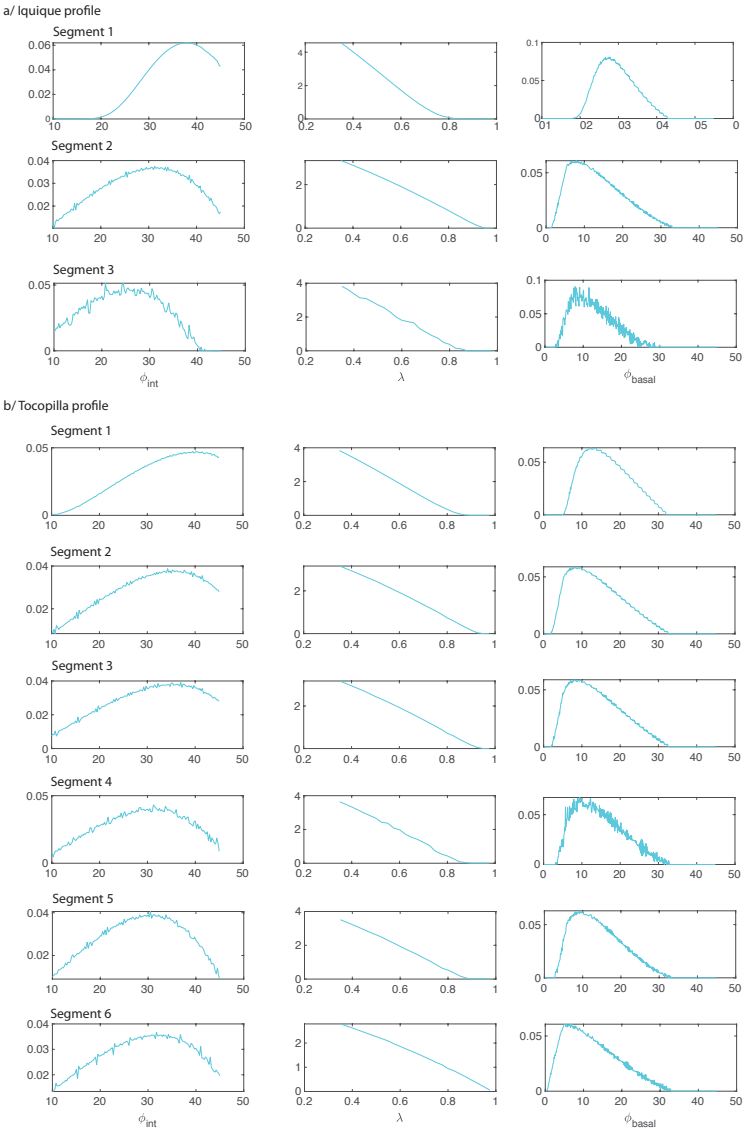

Figure 3: **S3 -** Marginals 1D obtained for Figure **2** profiles.

Table 1: **T1 -** Best misfits of critical segments identified on figures **2** and **S2** (δ_b: angle between forward verging thrust and basal décollement).

Cross-section	Internal pore pressure ratio λ	Internal friction angle ϕ_{int} (^{o})	Effective basal friction angle ϕ_b^{eff} (^{o})	Diff. of effective friction $\Delta\phi$ (^{o})	Diff. of dip δ_b (^{o})
Iquique					
1	0.35	33.75	22	1.47	8.1
2	0.775	35.5	8.8	0.3	5.8
3	0.35	27.25	17.0	0.15	9.8
Tocopilla					
1	0.7	42.25	14.7	0.54	5.3
2	0.85	41.5	7.4	0.16	4.1
3	0.5	32.5	16.0	1.67	9.7
4	0.35	40.5	28.7	0.33	3.4
5	0.625	31.75	12.6	0.46	6.2
6	0.775	38.75	9.8	0.43	6.1
Antofagasta					
1	0.475	30.75	15.4	1.94	10.8
Illapel					
1	0.625	38.75	15.1	1.65	9.0
2	0.575	27.75	12.5	0.1	3.2
3	0.575	25.25	11.2	0.13	6.4
4	0.575	25.25	11.2	0.13	6.4
Maule					
1	0.35	27.25	12	6.	19
2	0.575	39.75	16.8	2.67	10.3
3	0.4	30.75	15.6	4.04	14.3
4	0.5	27.25	13.6	0.84	8.2
5	0.65	29.0	10.5	0.48	7.0
6	0.6	37.25	16.8	0.12	2.7
7	0.525	26.5	13	0.32	5.5

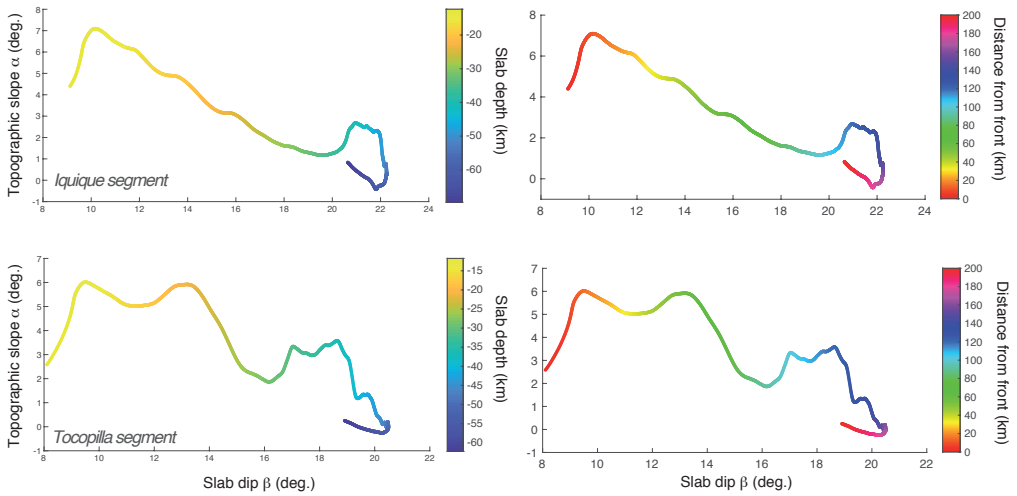

Figure 4: **S4 -** Topographic slope (α) versus slab dip (β) of Figure **2b** and **2c** profiles with depth evolution and distance from the front shown as a gradient of color.

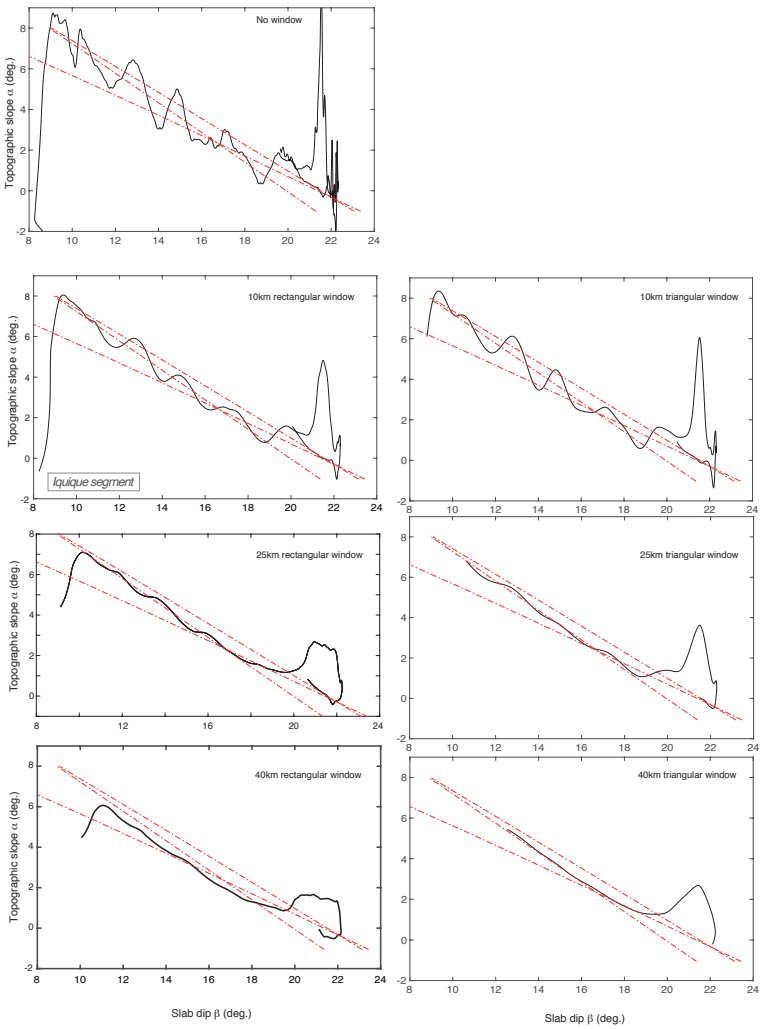

Figure 5: **S5 -** Figure **2b** profile, original and smoothed topography by different window size (10, 25 and 40 km) and shape (rectangular, triangular). The critical areas are visible on original and smoothed data for both window shapes. The 25km large window allows keeping some topographic complexities and is smoothed enough to capture critical areas.

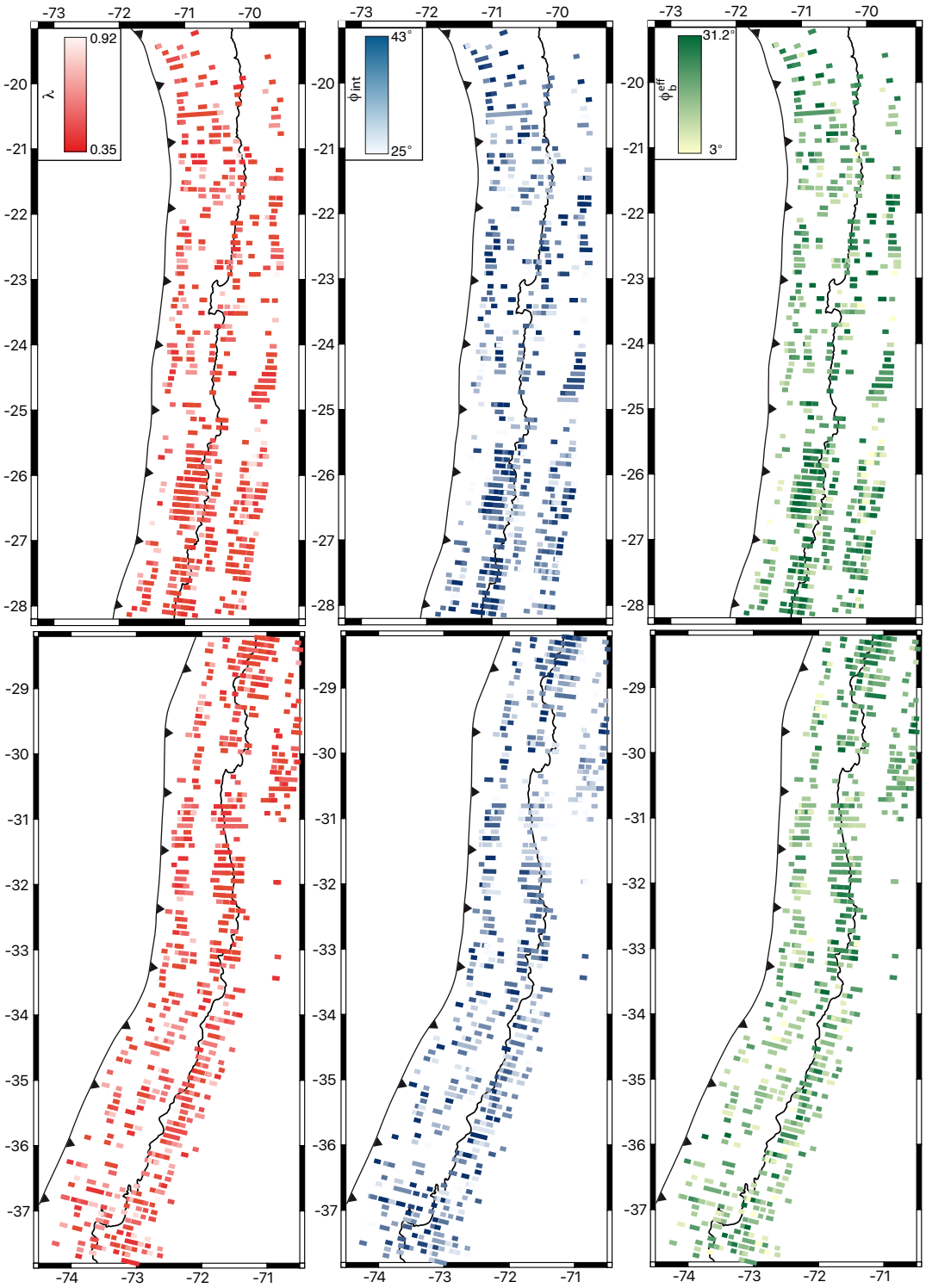

Figure 6: **S6** - Frictional properties of segments at critical state retrieved by inversion: Best misfits for internal pore pressure, internal friction angle and effective megathrust friction angle.

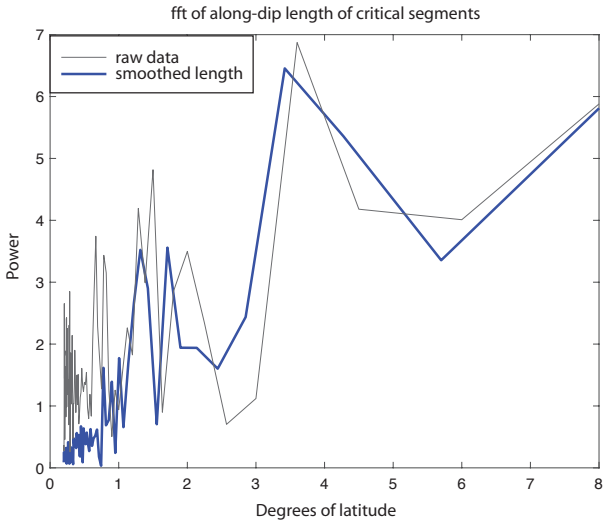

Figure 7: **S7** - FFT applied on raw and smoothed lengths of segments at critical state, as a function of latitude degrees. We can identify four major peaks: 8, 4, 2, 1.5^o

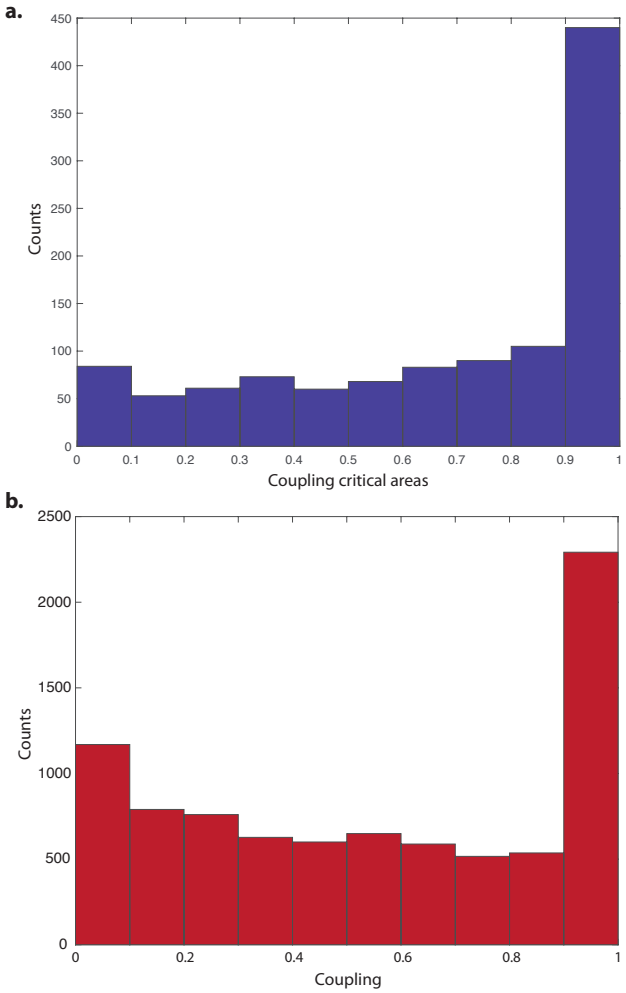

Figure 8: **S8** - Histograms of coupling values for a. critical segments and for b. Metois et al. (2016) model Metois et al. (2016)

References

M. Metois, C. Vigny, A. Socquet, Interseismic coupling, megathrust earthquakes and seismic swarms along the chilean subduction zone (38–18 s), Pure and Applied Geophysics 173 (2016) 1431–1449.